ANALYSIS AND EVALUATION OF BRIDGE DAMAGES USING HIGH-RESOLUTION SAR IMAGERY

Kazuki Inoue[1], Wen Liu[1], Marc Wieland[2], Tadashi Sasagawa[3], and Fumio Yamazaki[1]

[1] Chiba University, 1-33 Yayoi-cho, Inage-ku, Chiba 263-8522, Japan.
Email: kinoue@chiba-u.jp; wen.liu@chiba-u.jp; fumio.yamazaki@faculty.chiba-u.jp
[2]GFZ German Research Centre for Geosciences, 14467 Potsdam, Germany. Email: mwieland@gfz-potsdam.de
[3]PASCO Corporation, Tokyo 153-0043, Japan. Email: taawda5004@pasco.co.jp

KEY WORDS: Tsunami, TerraSAR-X, Bridge, Damage Assessment, The 2011 Tohoku Earthquake

ABSTRACT: After the M_w 9.0 Tohoku Earthquake on March 11, 2011, many bridges were damaged severely due to the tsunamis caused by the earthquake. Since the road network was fragmented, it was difficult to grasp the level of damage by field surveys alone. In order to provide emergency response quickly after an earthquake, the extraction of damaged areas at an early stage is very important. In this context, satellite images are useful for detecting damages over large areas after disasters. The objective of this study is to collect the damage information quickly by analyzing satellite images. SAR images, which can be obtained in cloudy weather or nighttime, were adopted in this study. TerraSAR-X images covering Sendai, Miyagi Prefecture, Japan, which were acquired on October 21, 2010 (pre-event), March 13 and 24, 2011 (post-event) were used for change extraction and analysis of bridge damages. The characteristics of the backscattering intensity were investigated by comparing with the damage situation. For collapsed bridges or scored embankments, it can be expected that the SAR backscatter decreases from the pre-event image to the post-event one, and the level of damage can be extracted by proper threshold values of backscatter and the results were compared with aerial/satellite optical images.

1. INTRODUCTION

After an earthquake strikes, the road network is often fragmented, or the transportation systems are paralyzed. Therefore, it is difficult to grasp the level of damage by field surveys alone. In the 1994 Northridge earthquake with M_w 6.7, which occurred on January 17 PST in Los Angeles, California, United States, many transportation structures were severely damaged. Major roads and freeways were closed because of structural failure or collapse, and especially, the most notable damage was the collapse of a bridge on Interstate 10. Similarly, in the Kobe earthquake with M_w 6.8, which occurred on January 17, 1995 JST in Hyogo Prefecture, Japan, many civil engineering structures were severely damaged such as collapsed elevated highways (e.g., Hanshin Expressway) and elevated railroads (e.g., Sanyo Shinkansen).

Furthermore, in the 2011 earthquake off the Pacific coast of Tohoku with M_w 9.0, which occurred on March 11, 2011 JST, the function of many local public bodies having prime responsibility for emergency response was lost due to the widely extended disaster. At the same time, the operational capabilities of field surveys were limited due to increased danger for the operators and due to the large area covered by the disaster. In order to provide emergency response quickly after an earthquake, the extraction of damaged areas at an early stage is significant. At this point, analyzing damages using remote sensing, which can collect data on dangerous or inaccessible areas, is a useful alternative. In addition, highly accurate information on the level of damage is retrieved by using remote sensing and field surveys together in a complementary way. In remote sensing methods, compared with optical sensors, synthetic aperture radar (SAR) does not suffer from the limitation of sunlight, weather conditions, and fire smoke. Thereby, it is useful in emergency response immediately after a disaster strikes.

A number of studies exist on the topic of damage detection from remote sensing. Hasegawa et al. (2000) studied the extraction of building damages in the 1995 Kobe earthquake using aerial images, and estimated the accuracy of damage classification from them. Maruyama et al. (2006) interpreted road damages after the 2004 Mid-Niigata earthquake using aerial photographs and analyzed the effect of the spatial-resolution of imagery in damage extraction. Miura et al. (2013) investigated on the interpretation of building damages after the 2006 Central Java earthquake using high-resolution optical satellite images. Shoji et al. (2012a, b) studied on the collapsed or washed-away girders and eroded approach-embankments of bridges due to the tsunamis caused by the 2011 Tohoku earthquake using optical satellite images from Google Earth and compared the results with the damage data by field surveys. Liu et al. (2013) studied on the extraction of flooded areas and building damages after the 2011 Tohoku earthquake using the pre- and post-event TerraSAR-X images.

Since only few studies exist on the damage assessment of bridge structures due to earthquakes or tsunamis, especially from SAR imagery, this paper investigates the capability of high-resolution SAR imagery in bridge damage detection due the 2011 Tohoku earthquake. Four collapsed bridges as well as six non-damaged bridges in Miyagi prefecture, Japan, within the TerraSAR images are examined using pre- and post-event imagery data. The damage situations of the bridges are inferred first by a color-composite of the two-temporal SAR images. Then the change of the backscattering coefficient in the surrounding area of a bridge is examined in terms of the difference and the correlation coefficient and the result is compared with field reports and optical aerial/satellite images.

2. THE STUDY AREA AND IMAGERY DATA

Figure 1 show the study area including the damaged (or washed-away) and non-damage bridges and the color composite of three-temporal TerraSAR (TSX) images covering the Sendai and Ishinomaki Planes, Miyagi Prefecture, Japan, which were acquired on October 21, 2010 (pre-event), March 13, 2011 (two days after the earthquake), and March 24, 2011 (13 days after the earthquake) in the local time. These images were used in the authors' previous papers on the extraction of crustal movements (Liu and Yamazaki, 2013) and the evaluation of flooded areas and building damages (Liu et al., 2013). We assign red color for the pre-event image and cyan (blue + green) color for the post-event one, in order to observe the changes in SAR backscatter. As a result, if the color composite exhibits a dominant color, it indicates a stronger backscatter for that colored SAR image. Owing to this, the damage situation of an individual bridge can be visually observed.

The incident angle of the SAR data was about 37.30°, and the heading angle was about 190.29°, from the descending path. All the images were taken in the StripMap mode with the HH polarization. The azimuth and ground-range resolutions were about 3.0 m. After the enhanced ellipsoid correction (EEC), the images were transformed into the pixel size of 1.25 m.

Three pre-preprocessing steps were applied to all the images. First, the images were transformed from digital numbers (DN) to backscattering coefficients (sigma naught; σ^0), which represent the radar reflectivity per unit area in the ground range. Second, an Enhanced Lee filter (Lopes et al., 1990) was applied to the original TSX images to reduce the speckle noises. In order to minimize any loss of information included in the intensity images, the window size of the filter was set to 3 × 3 pixels.

Third, the coseismic and post-seismic displacements (Ozawa et al., 2011) due to the M_w9.0 mega earthquake were removed. The shift for the post-event TSX images with respect to the the pre-event one was estimated as 3.11 m to the east and 0.55 m to the south in the Sendai area. Thus, the pre-event TSX image was manually shifted 2 pixels (2.5 m) to the east and 1pixel (1.25m) to the south in order to register with the post-event TSX images (Liu et al., 2013).

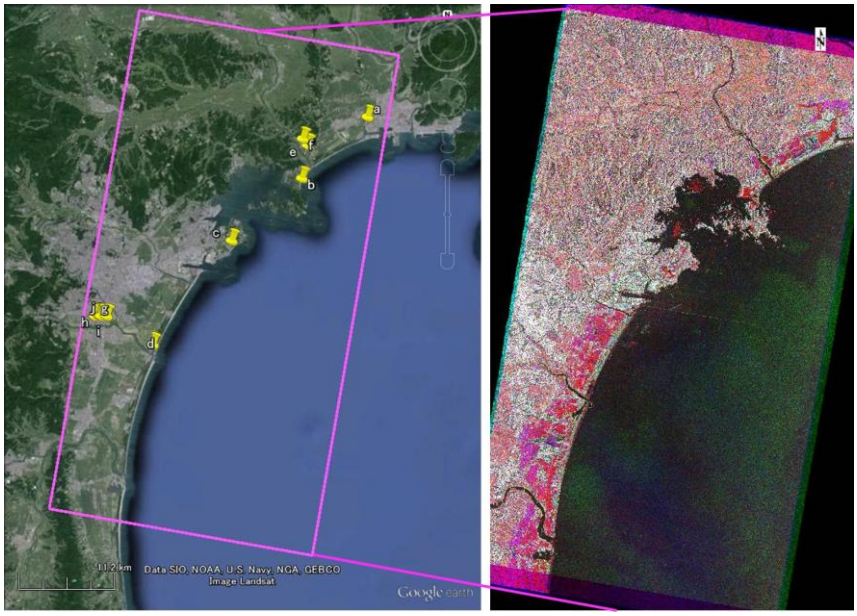

(a) The study area with bridge locations (b) The color-composite

Figure 1. The study area (a) and the color-composite of TerraSAR-X imagery data (b)

3. EXAMINATION OF SAR IMAGES FOR BRIDGES

The objective of this research is to examine SAR intensity images before and after the tsunami attack, and then identify the characteristics of the SAR backscatter representing the damage status of bridges. In the TSX imaging area, four collapsed or washed-away bridges were located based on Shoji et al. (2012a, b). The damage situations of the bridges were also referred from several reports (Joint Survey Group of Tohoku Branches of Academic Societies, 2013). For a comparison purpose, six bridges without suffering severe damage were also selected in the imaging area shown in **Figure 1**. In order to observe the status of the target bridges well in the color-composite images, the backscattering coefficients of the original TSX images were set in the range between -35 dB to -10 dB.

Change images from the two-temporal TSX intensity images have been compiled using the difference value, d, and the correlation coefficient value, r, as follows,

$$d = \bar{Ia}_i - \bar{Ib}_i \tag{1}$$

$$r = \frac{N\sum_{i=1}^{N} Ia_i Ib_i - \sum_{i=1}^{N} Ia_i \sum_{i=1}^{N} Ib_i}{\sqrt{\left(N\sum_{i=1}^{N} {Ia_i}^2 - \left(\sum_{i=1}^{N} Ia_i\right)^2\right)\cdot\left(N\sum_{i=1}^{N} {Ib_i}^2 - \left(\sum_{i=1}^{N} Ib_i\right)^2\right)}} \tag{2}$$

where i is the pixel number, Ia_i and Ib_i are the backscattering coefficients of the prost-event and pre-event images, respectively, $\bar{Ia}_i$ and $\bar{Ib}_i$ are the corresponding averaged values over the N ($= k \times k$) pixels window surrounding the i-th pixel. The window size, N, may be assigned by considering the spatial resolution of the SAR images and the size of target objects. In this study, we set them as 9 x 9 pixels, which is equal to a ground-coverage of 126.6 m^2.

In order to make visual interpretation easier, the difference and the correlation coefficient values were plotted by superposing on the pre-event image. Proper threshold values for the difference and correlation coefficient were sought in order to extract collapsed bridges. For evaluation, the results were compared with aerial photos by the Geospatial Information Authority of Japan (GSI, 2015) and optical satellite images from Google Earth.

3.1 Jogawa Bridge

First, Jogawa Bridge (141.247E, 38.420N), a post-tension PC (pre-stressed concrete) girder bridge connecting Higashi-Matsushima and Ishinomaki Cities over Jogawa River, was investigated as shown in **Figure 2**. The total length of the bridge was 126.0 m with three spans of 41.03 m each. The bridge was classified as collapse (B4) by Shoji et al. (2012a, b). As seen in the aerial image in **Figure 2(a)**, the bridge girder of the center span fell down and washed away to the north by the tsunami. Due to this damage, the backscattering coefficient for the collapsed girder was decreased as seen in **Figure 2(b)** and **(c)** while the side girders were left and seen to be no much change. Since the piers were left in the river, they showed point-like strong backscatter. The correlation coefficient in **Figure 2(d)** became low for the collapsed section but almost no change for the remaining sections of the bridge. The damage situation of the river embankments are also clearly observed in both the SAR and optical images. Hence the apparent damage like this bridge can be easily extracted from high-resolution SAR intensity images.

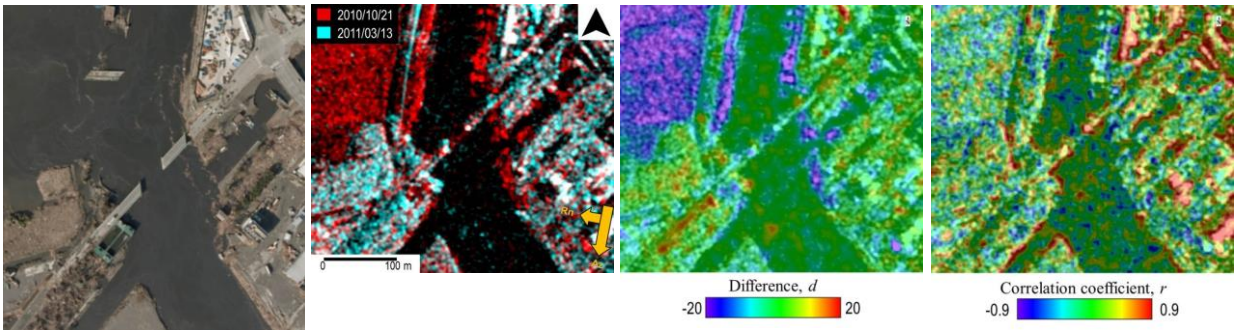

(a) Optical image (b) Color composite (c) Difference (d) Correlation coefficient

Figure 2. Close-up of Jogawa Bridge area. The optical image taken by GSI on 12 March 2011 (a), the color-composite (b), the difference (c), and the correlation coefficient of the pre- and post-event TSX images.

3.2 Matsugashima Bridge

Matsugashima Bridge (141.157E, 38.354N), a post-tension PC girder bridge in Higashi-Matsushima City connecting Miyato Island and the main land, was also collapsed by the tsunami as seen in **Figure 3**. The total length of the bridge was 45.5 m with three spans of 14.55 m each. According to the report (Joint Survey Group of Tohoku Branches of Academic Societies, 2013), the soil embankments behind the two abutments were eroded and mostly washed away. But the three-span main girder was shifted but remained without falling down.

The backscattering coefficient of the collapsed section (the embankment behind the south abutment) is seen to decrease while that of the central part to increase as shown in **Figure 3(b)**. Comparing with the optical image, it was observed that the debris brought by the tsunami was remained at the central part. The difference and the correlation coefficient were also calculated for this bridge area. As seen in **Figure 3(c)** and **(d)**, the reduced difference and correlation were observed in the collapsed section. On the contrary, the difference was unchanged and the correlation coefficient was kept high for the survived parts of the bridge.

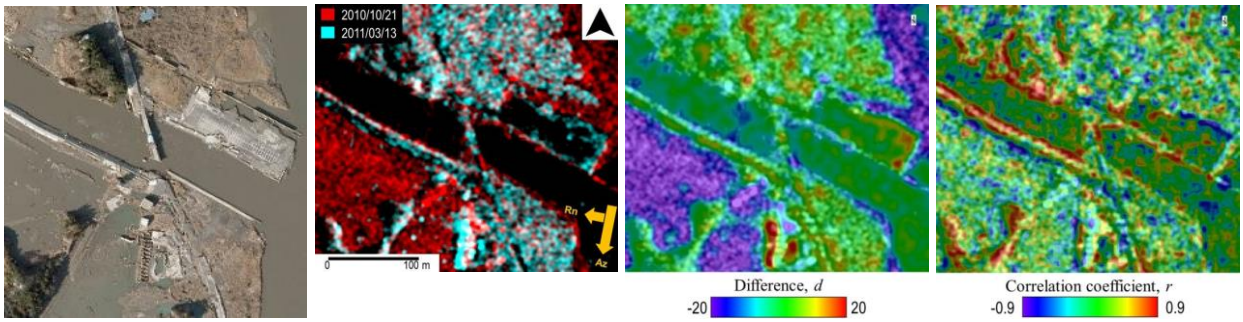

(a) Optical image (b) Color composite (c) Difference (d) Correlation coefficient

Figure 3. Close-up of Matsugashima Bridge area. The optical image taken by GSI on 12 March 2011 (a), the color-composite (b), the difference (c), and the correlation coefficient of the pre- and post-event TSX images.

3.3 Hashimoto Bridge

Hashimoto Bridge (141.061E, 38.287N) on Miyagi Prefectural Road No. 58, located in Shichigahama Town, was also investigated because this bridge was classified as collapsed (B4) together with nearby Niramori Bridge by Shoji et al. (2012a, b). The length of the bridge was estimated 7.1 m from optical images. Hayashikawa et al. (2011) reported that the bridge was made of box culvert and the bridge was displaced but not much damaged by the tsunami although the backfill soil of the culvert was highly scored.

Figure 4 shows the area including Hashimoto Bridge. From the aerial photos by the GSI, the bridge was confirmed still flooded by water and almost covered by debris on March 13, 2011 (the post-event TSX) and it was difficult to recognize the bridge from the SAR image. Thus, another TSX image acquired on March 24, 2011 was used as the post-event SAR image. From the optical image acquired on April 6, 2011 shown in **Figure 4 (a)**, this bridge was seen to be temporarily restored at that time.

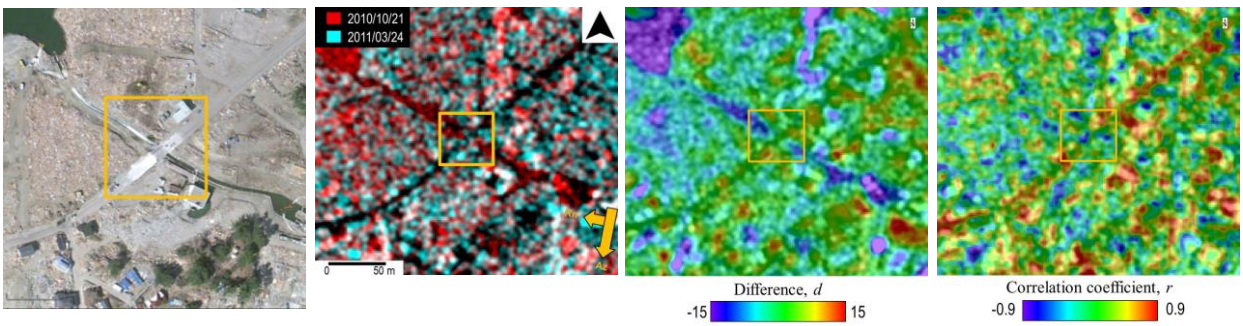

(a) Optical image (b) Color composite (c) Difference (d) Correlation coefficient

Figure 4. Close-up of Hashimoto Bridge area. The optical image from Google Earth on 6 April 2011 (a), the color-composite (b), the difference (c), and the correlation coefficient of the pre- and post-event TSX images.

The backscattering coefficient at the both ends of the bridge is seen to decrease slightly although it is not so clear in **Figure 4(b)**. Subsequently, the difference value has no significant change at the location of the bridge. However, the correlation coefficient values got smaller for the bridge location, and kept high along the survived road. Since for the bridge was small, it was difficult to extract the range of the bridge.

3.4 Miyashita Bridge

Miyashita Bridge (140.955E, 38.177N) was located near the mouth of the Natori River, crossing Teizan-bori Canal together with the nearby water gate, as shown in **Figure 5**. The length of the main girder was 26.1m (estimated). It was classified as bridge collapse (B4) by Shoji et al. (2012a, b). It was reported that the main girder fell down and the attached pipes and their supporting piers were collapsed. The approach's embankment was eroded severely. **Figure 5 (b)** shows that the backscattering coefficients of the pipes, piers and embankments decreased and those of the bridge and floodgate had no much change between the pre- and post-event images. Since the bridge was rather small and the girder remained after it fell down, the extraction of changes in the SAR images from the difference and the correlation coefficient is considered not so easy.

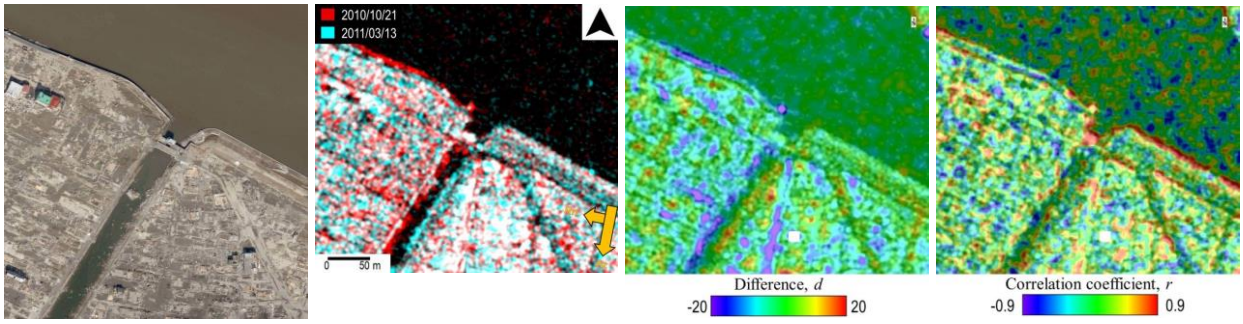

(a) Optical image (b) Color composite (c) Difference (d) Correlation coefficient

Figure 5. Close-up of Miyashita Bridge area. The optical image taken by GSI on 13 March 2011 (a), the color-composite (b), the difference (c), and the correlation coefficient of the pre- and post-event TSX images.

3.5 Two Bridges over Naruse River

Narusegawa Railway Bridge (141.165E, 38.389N, length 489 m) of the JR Sendai-Ishinomaki Line and Naruse-ohashi Bridge (141.158E, 38.396N, length 435 m) on the National Highway No. 45 were investigated as samples of non-damaged bridges (**Figure 6**). The both bridges were located in Higashi-matsushima City, at 2 - 3 km from the mouth of the Naruse River. The tsunami intruded the land in the both sides of the bridges as seen in red in the color composite **(b)**, but these bridges were located in higher altitude than the tsunami water level and thus they did not suffer from significant damage. The difference **(c)** and the correlation coefficient **(d)** from the pre- and post-event TSX images show no significant changes for the pixels including the bridges.

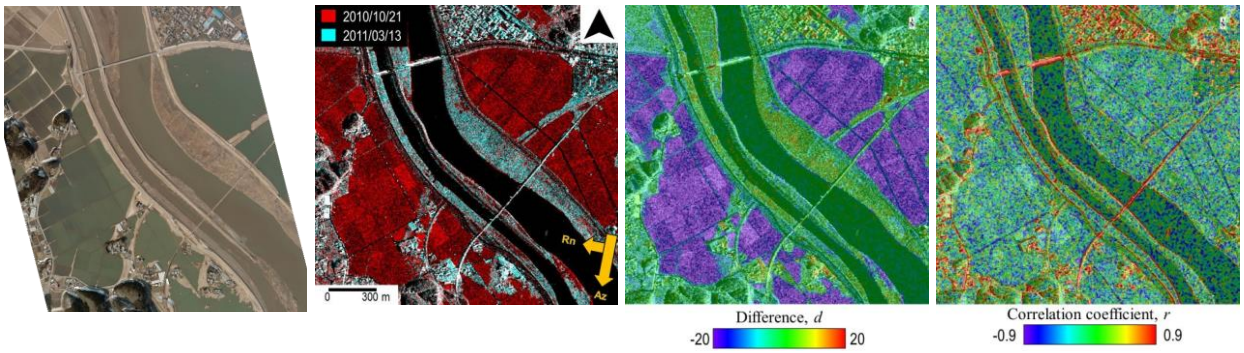

(a) Optical image (b) Color composite (c) Difference (d) Correlation coefficient

Figure 6. Close-up of the area including Narusegawa Railway and Naruse-ohashi Bridges. The optical image taken by GSI on 12 March 2011 (a), the color-composite (b), the difference (c), and the correlation coefficient of the pre- and post-event TSX images.

3.6 Four Bridges over Natori River

The situation of four bridges shown in **Figure 7** over the Natori River in Sendai City were studied, namely Taihaku-ohashi Bridge (140.877E, 38.206N, length 625 m) on Miyagi Prefectural Road No. 258, Natorigawa Railway Bridge (140.883E, 38.207N, length 620 m) of JR Tohoku and Tohoku-Shinkansen Lines, Natori Bridge (140.885E, 38.206N, length 475 m) on the National Highway No. 4, and Natori-ohashi Bridge (140.892E, 38.207N, length 539 m) on the Sendai Bypass. Although the tsunami went up the Natori River more than the bridge locations, these bridges were basically not affected by the tsunami. The color-composite **(b)** shows that the backscatter of the pixels around the bridges did not change by the event because they are shown in white color. The difference **(c)** and the correlation coefficient **(d)** from the pre- and post-event TSX images show no significant changes for the pixels including the bridges.

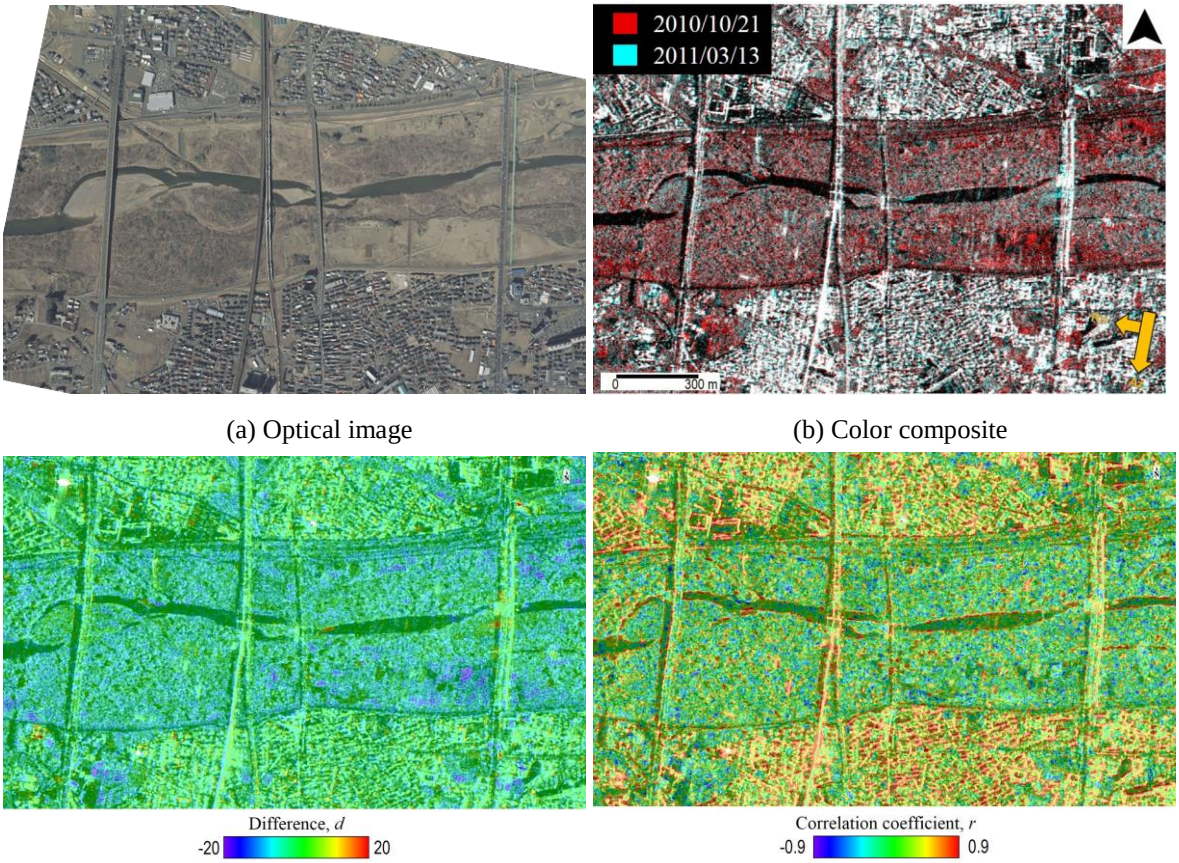

(a) Optical image (b) Color composite

(c) Difference (d) Correlation coefficient

Figure 7. Close-up of the area including Taihaku-ohashi, Natorigawa Railway, Natori, and Natori-ohashi Bridges. The optical image taken by GSI on 12 March 2011 (a), the color-composite (b), the difference (c), and the correlation coefficient of the pre- and post-event TSX images.

4. COMPARISON OF DIFFERENCE AND CORRELATION BETWEEN COLLAPSED AND NON-DAMAGED BRIDGES

Next, the difference and the correlation coefficient of the backscatter between the pre- and post-event SAR images were examined in more detail for the four affected bridges and six non-damaged ones. To assess the change for each bridge area, the range of evaluation was determined as the footprint of the bridge as shown in **Figure 8**. Then we extracted the range of the sigma naught values (max, min) and the mean value for the difference and the correlation coefficient, and compared the change of the mean value between the two time-instants.

Table 1 shows the range and the mean value of the difference (d) and the correlation coefficient (r) for the ten bridges described previously. The mean values of d and r for each bridge area are also compared in **Figure 9**. It is observed from the figure that the mean of the difference for the bridge footprint is smaller than -2.0 dB for the

damaged bridges (a, b, d) except for that of Hashimoto Bridge (c) while the mean value is in the range -2.0 dB to 2.0 dB for the non-damaged bridges (e-j). Hashimoto Bridge showed the different tendency with the other collapsed bridges because it was short and the bridge was covered by debris. Debris is usually considered to have stronger backscatter than bridge structures. The difference of the sigma naught values is considered to be small for non-damaged bridges because of no significant change in backscatter.

The mean value of the correlation coefficient is high for the two non-damaged bridges (e, f), but it is almost the similar value with those of the collapsed bridges (a, b, d) for the other four non-damaged bridges (g-j). This observation was probably caused by several reasons. First, the traffic condition might affect the correlation coefficient because the non-damaged bridges might be crowded with cars and trucks. The length of the collapsed section and the length of the bridge also affect the correlation. Thus when calculating the mean value for a bridge, we must be careful on the range of the averaging.

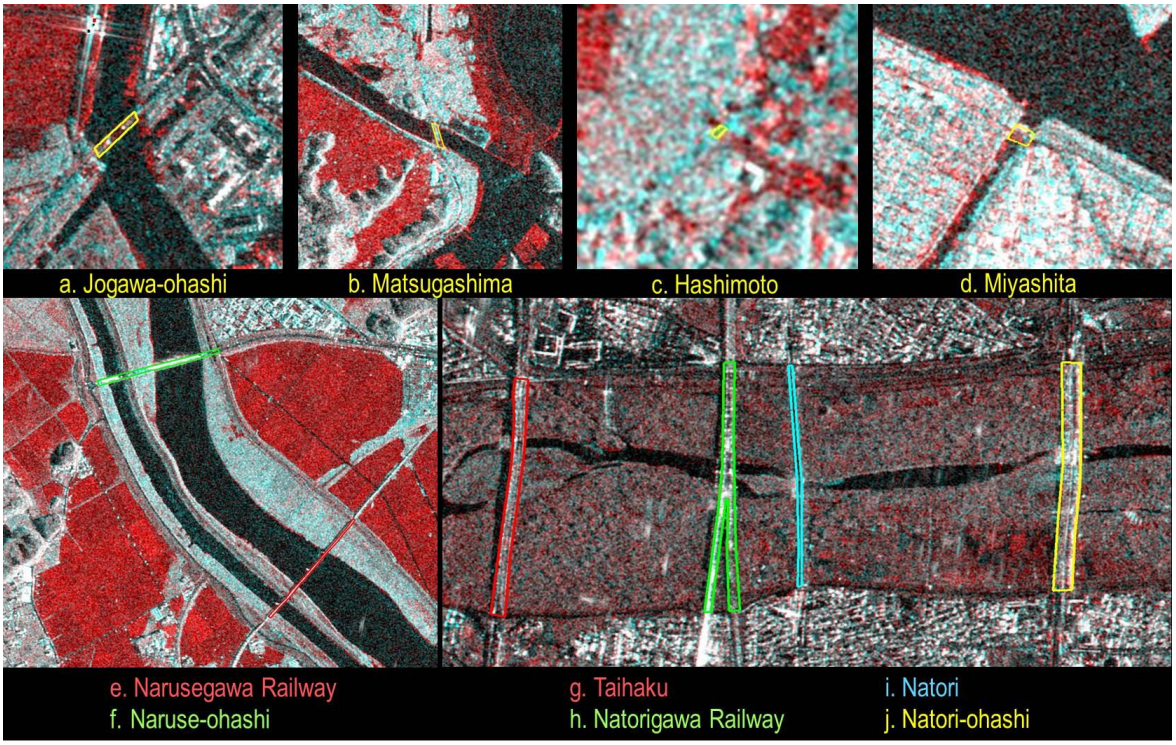

Figure 8. Ranges of extracting the difference and correlation-coefficient values of the bridges.

Table 1 The range and the mean value of the difference *d* and the correlation coefficient *r* for the ten bridges

Damage Situation	Bridge Name	Symbol	Difference, *d*			Correlation Coefficient, *r*		
			Min	Max	Mean	Min	Max	Mean
Collapsed	Jogawa-ohashi	*a*	-14.49	7.31	-3.70	-0.69	0.88	0.41
	Matsugashima	*b*	-19.34	10.60	-2.25	-0.54	0.83	0.17
	Hashimoto	*c*	1.08	8.95	4.92	-0.73	-0.07	-0.36
	Miyashita	*d*	-13.64	9.42	-4.79	-0.67	0.91	0.19
Non-damaged	Narusegawa Railway	*e*	-6.84	10.95	1.96	-0.78	0.98	0.72
	Naruse-ohashi	*f*	-8.18	24.90	2.04	-0.78	0.99	0.69
	Taihaku	*g*	-13.28	9.64	-0.96	-0.79	0.90	0.21
	Natorigawa Railway	*h*	-12.81	11.33	-0.49	-0.58	0.94	0.43
	Natori	*i*	-8.79	7.57	-1.21	-0.56	0.92	0.37
	Natori-ohashi	*j*	-15.99	16.04	-0.38	-0.77	0.91	0.31

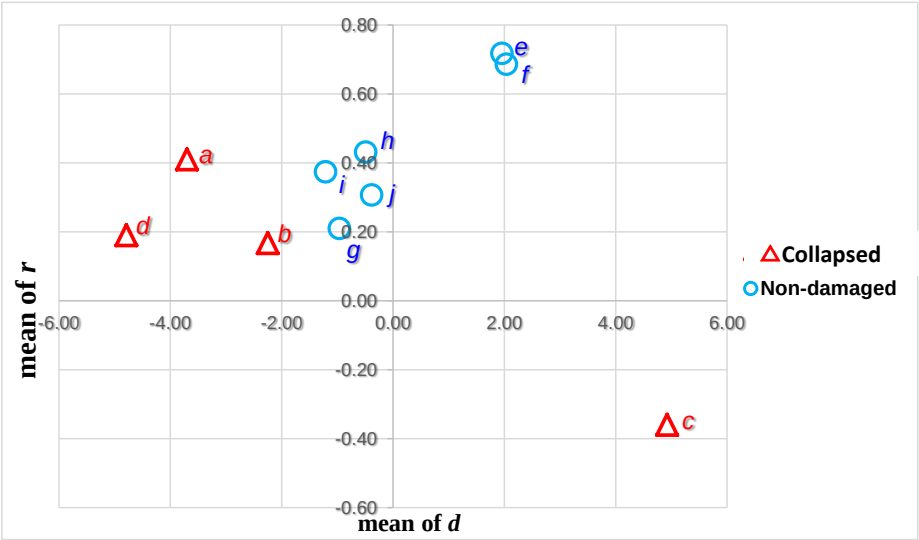

Figure 9. The relationship between the mean values of *d* and *r* for the areas of bridge footprints

Although the number of data points is still not enough, there is a possibility to classify collapsed and non-damaged bridges from the SAR backscattering characteristics if we have pre- and post-event SAR images of bridges from the same acquisition condition. Even if no pre-event image exits, a post-event image of higher-resolution mode (Spot Light) enables damage extraction of structures only from a single image (Dell'Acqua and Polli, 2011).

For Naruse-ohashi Bridge, the bridge itself was not damaged, but bumps of pavement developed by the subsidence of the river embankment. The present method is not applicable to extract bumps, but InSAR method can be used to extract settlements and displacements. The preparation of bridge inventory database is necessary for future earthquakes and tsunamis. If such a database is prepared, post-event SAR data may be efficiently used to assess damage situation of the bridges in affected areas, and then to plan for emergency response operations.

5. CONCLUSIONS

The 2011 Tohoku Earthquake tsunami caused significant effects to transportation networks along the Pacific coast of the eastern Japan. A large number of road and railway bridges were collapsed and some of bridge girders were washed away by the tsunami. The backfill of bridge abutments and river embankments were scored and some bridges became inaccessible. In this paper, the capability of high-resolution SAR imagery in bridge damage detection was investigated using pre- and post-event TerraSAR-X imagery data. Four collapsed bridges and six non-damaged bridges in Miyagi Prefecture, Japan, within the TerraSAR imaging area were selected and examined visually first by color-composite of the two-temporal images. Then the change of the backscattering coefficient in the bridge footprint was investigated in terms of the difference and the correlation coefficient. Comparing these results with field survey reports and optical aerial/satellite images, capability of high-resolution SAR images in bridge damage extraction was demonstrated. By setting threshold values for the difference and correlation coefficient for the bridge area, the damage situation of the bridge can be estimated properly if the bridge and its damaged portion are large enough and in the sight of radar illumination. But we still need to accumulate validation data until a solid conclusion is drawn.

ACKNOWLEDGEMENTS

The TerraSAR-X images used in this study were provided by PASCO Corporation, Tokyo, Japan, as one of the granted projects of the SAR data application research committee in 2011. The TerraSAR-X data are owned by the German Aerospace Center (DLR) and the copyright belongs to Infoterra GmbH. This research was financially supported in part by the Grant-in-Aid for Scientific Research from Ministry of Education, Culture, Sports, Science, and Technology (MEXT) under the Grant No. 24241059.

REFERENCES

Dell'Acqua, F., Polli, D.A., 2011. Post-event only VHR radar satellite data for automated damage assessment: a study on COSMO/SkyMed and the 2010 Haiti earthquake, Photogrammetric Engineering & Remote Sensing, 77(10), pp. 1037-1046.

Geospatial Information Authority of Japan. GSI Maps. Retrieved July 20, 2015, from http://maps.gsi.go.jp/.

Hasegawa, H., Yamazaki, F., Matsuoka, M., Sekimoto, I., 2000. Determination of building damage due to earthquakes using aerial television images, 12th World Conference on Earthquake Engineering, CD-ROM, 8p.

Hayashikawa et al. 2011. Damage survey report on bridges, Retrieved August 23, 2015, from http://www.eng.hokudai.ac.jp/labo/bridge/news/20110808%20earthquake/2011Earthquake%20Investigation.pdf

Joint Survey Group of Tohoku Branches of Academic Societies, 2013. Survey Report on the 2011 Tohoku Earthquake, 498p.

Lopes, A., Touzi, R., Nezry, E., 1990. Adaptive speckle filters and scene heterogeneity. IEEE, Trans Geosci Remote Sens 28(6), pp. 992–1000.

Liu, W., Yamazaki, F., 2013. Detection of crustal movement from TerraSAR-X intensity image. IEEE, Geosci Remote Sens Lett 10(1), pp. 199-203.

Liu, W., Yamazaki, F., Gokon, H., Koshimura, S., 2013. Extraction of tsunami-flooded areas and damaged buildings in the 2011Tohoku-Oki Earthquake from TerraSAR-X intensity images. Earthquake Spectra, 29(S1), pp.183-200.

Maruyama,Y., Yamazaki, F., Yogai, H., Tsuchida,Y, 2006. Damage detection of expressways in the 2004 Niigata-Ken Chuetsu earthquake using aerial photographs, Proceedings of the 2nd Asia Conference on Earthquake Engineering, Manila, Philippines, CD-ROM, Paper No.IVC2, 11p.

Miura, H., Midorikawa, S. and Kerle, N., 2013. Detection of building damage areas of the 2006 Central Java, Indonesia earthquake through digital analysis of optical satellite images, Earthquake Spectra, 29(2), pp.453-473.

Ozawa, S., Nishimura, TH., Suito, H., Kobayashi, T., Tobita, M., Imakiire, T., 2011. Coseismic and postseismic slip of the 2011 magnitude-9 Tohoku-Oki earthquake. Nature 475 (7356), pp.373–377.

Shoji, G., Takahashi, K., Nakamura, T., 2012a. Tsunami damage assessment on bridge structures subjected to the 2011 off the Pacific coast of Tohoku earthquake tsunami. JAEE, Vol. 12, No. 6, pp. 104-191 (in Japanese).

Shoji, G., Nakamura, T., Takahashi, K., Sakurai, T., 2012b. Tsunami damage assessment on road structures in the 2011 off the Pacific coast of Tohoku earthquake. JSCE, Vol. 68, No.4, pp.I_1186-I_1193.